Microglial and neuronal cell pyroptosis induced by oxygen-glucose deprivation/reoxygenation aggravates cell injury via activation of the caspase-1/GSDMD signaling pathway

Zhaofei Dong
Sun Yat-sen Memorial Hospital, Sun-Yat-sen University
Qingxia Peng
Sun Yat-sen Memorial Hospital, SunYat-sen University
Kuang Pan
Sun Yat-sen Memorial Hospital, Sun Yat-sen University
Weijye Lin
Sun Yat-sen Memorial Hospital, Sun Yat-sen University
Yidong Wang (wydys@126.com)
Sun Yat-sen Memorial Hospital,Sun Yat-sen University

Research

Keywords: pyroptosis, neuron, microglia, oxygen-glucose deprivation/reoxygenation (OGD/R), inflammation, Gasdermin D (GSDMD), Necrosulfonamide

Posted Date: February 24th, 2020

DOI: https://doi.org/10.21203/rs.2.24263/v1

Abstract

Background Pyroptosis is a new type of programmed cell death, which induces a strong pro-inflammatory reaction. However, the mechanism of pyroptosis after brain ischemia/reperfusion (I/R) and the interaction between different neural cells are still unclear. This study comprehensively explored the mechanisms and interactions of microglial and neuronal pyroptosis in the simulated I/R environment in vitro.

Methods The BV2 and HT22 cells were treated by oxygen-glucose deprivation/reoxygenation (OGD/R). The pyroptotic cells were detected by dye uptake method. The expression levels of pyroptotic-related proteins were determined by western blotting, immunofluorescence and enzyme linked immunosorbent assay. The cell viability was assessed using MTT assay Kit. AC-YVAD-CMK, necrosulfonamide and the siRNA of Gasdermin D (GSDMD) were used to observe the inhibited effect on caspase-1 and GSDMD, respectively. A transwell co-culture model was applied to observe pyroptosis and interactions between BV2 and HT22 cell after OGD/R.

Results Both BV2 and HT22 cells underwent pyroptosis after OGD/R, and the pyroptosis occurred at earlier time point in HT22 than that of BV2. Caspase-11 and Gasdermin E (GSDME) expression in BV2 and HT22 cells did not change significantly after OGD/R. Inhibition of caspase-1 or GSDMD activity, or down-regulation of GSDMD expression, alleviated pyroptosis in both BV2 and HT22 cells after OGD/R. Transwell studies further showed that OGD/R-treated HT22 or BV2 cells aggravated pyroptosis of adjacent non-OGD/R-treated cells, which could be relieved by inhibition of caspase-1 or GSDMD.

Conclusions OGD/R induces pyroptosis of microglia and neuronal cells and aggravates cell injury via activation of caspase-1/GSDMD signaling pathway. Our findings suggest that caspase-1 and GSDMD may be therapeutic targets after cerebral I/R. Necrosulfonamide, a chemical inhibitor of GSDMD, may be a potential drug to prevent cerebral I/R-induced brain injury.

Background

Stroke is a disease with high morbidity and mortality worldwide. Ischemic stroke accounts for about 80% of neurovascular injury [1]. At present, the treatment strategy of acute ischemic stroke is to restore blood flow as soon as possible, including drug thrombolysis and mechanical thrombolysis [2, 3]. However, the short time frame for safe intervention is still limited for these treatments. It is estimated that less than 10% of patients with acute stroke benefit from revascularization treatments, because of delayed treatment can lead to worsened outcome[4], which be caused by reperfusion injury. An important mechanism of reperfusion injury is the inflammatory response following cerebral ischemia/reperfusion(I/R) [5]. However, the inflammatory response after cerebral I/R is a very complex process, which still needs to be explored.

Recent studies have shown that the inflammasomes within brain cells (including neurons, microglia and astroglia) play an important role in inflammatory response to brain I/R injury [6–9]. Activation of caspase-1, a component of inflammasomes, induces the processing of pro-inflammatory cytokines pro-

IL-1β and pro-IL-18 into their matured forms. Activated caspase-1 is also known to induce a lytic type of cell death called pyroptosis. When cells undergo pyroptosis, membrane pores with diameters of 10–20 nm are formed and water influx is driven by intracellular non-ionic osmolytes, which causes cells swelling, membrane rupture, the release of cellular contents, and finally cell death. Pyroptosis can induce a strong pro-inflammatory reaction [10–14]. Activation of Gasdermin D (GSDMD), one of the gasdermin proteins family, is necessary for activated caspase-1 to induce cell pyroptosis. The activated caspase-1 cleaves GSDMD between the N-terminal and C-terminal domains. The N-terminal domain of GSDMD (GSDMD-N) has pyroptosis-inducing activity and plays a decisive role in pro-IL-1β and pro-IL-18 processing and secretion [15–17]. The inflammasome/caspase-1/GSDMD pathway is called the canonical inflammasome pathway. GSDMD can also be activated by active caspase-11 (rodent-derived) or caspase-4/5 (human-derived) in the case of lipopolysaccharide action, known as the non-canonical inflammasome pathway [11]. In addition, recent studies showed that caspase-3, known as an indicator of apoptosis all the time, also induces secondary necrosis (pyroptosis) through activation of Gasdermin E (GSDME) [18–20].

Although some studies have suggested that activation of GSDMD and pyroptosis in microglia and neurons in simulated ischemic conditions in vitro [21–23], however, it is still unclear whether there is interplay between microglial and neuronal pyroptosis after I/R, which results in inflammatory propagation. Moreover, there isn't any report about activation of GSDME following cerebral I/R. This study comprehensively explores the mechanisms and interactions of microglial and neuronal pyroptosis during mimic I/R injury in vitro.

Materials And Methods

Cell culture

BV2 microglia and HT22 neurons were purchased from American Type Culture Collection (ATCC). BV2 cells and HT22 cells were grown in Dulbecco's Modified Eagle Medium (DMEM) HighGlucose (Gibco, Invitrogen, USA) with 10% fetal bovine serum (Gibco, Invitrogen, USA) and 1% penicillin/streptomycin (Gibco, Invitrogen, USA) at 37 °C in a 5 % CO2 atmosphere.

Oxygen-glucose deprivation/reoxygenation (OGD/R) model

In order to simulate cerebral I/R, the OGD/R model was constructed by replacing normal culture medium with glucose-free DMEM medium (Gibco, Invitrogen, USA), and then the cells was placed in a hypoxic incubator (Anoxomat Mark II, Mart Microbiology B.V, Netherlands) that contained a gas mixture of 1% O_2, 5% CO_2 and 94% N_2 for 4h (BV2 cells) or 2h (HT22 cells) at 37°Cand then recovering normal gas and culture medium at the optimal time. Samples collected at various time points after OGD/R for subsequent experiments. Normal cultured cells were used as the control group.

Experimental design

This study consisted of three parts．In part 1 experiment, proportion of pyropotic BV2 and HT22 cells． expression of pyroptosis-related protein and cell viability were observed during OGD/R (Figure 1a). Part 2 experiment explored the effect of inhibition of caspase-1 or GSDMD on BV2 and HT22 cell pyroptosis following OGD/R (Figure 1b). Part 3 experiment demonstrated the interaction of BV2 and HT22 cell pyroptosis after OGD/R by the transwell co-culture system (Figure 1c-1d).

Detection of cell pyroptosis by dye uptake

The dye uptake method was carried as previously reported [12]. When the cell increase in the uptake of YO-PRO-1 iodide, a small (629 Da) membrane impermeable dye, with exclusion of a larger (1293 Da) membrane impermeable dye, ethidium homodimer-2 (Eth-D2), it was considered as formation of discrete pores in the plasma membrane and defined as cells underwent pyroptosis. The cells at various time points after OGD/R in the culture dish of 10cm in diameter was added to 1uM YO-PRO-1 iodide (Invitrogen, Shanghai, China), 1uM Eth-D2 (Invitrogen, Shanghai, China) and 2uM Hoechst 33342 (Invitrogen, Shanghai, China) for 10min. Then wash the cells with PBS twice, 5min each. Triton X-100 detergent (0.1%) was used as a positive control for dye uptake. Normally cultured cells are treated as controls. Images were captured using a ZEISS A2 inverted microscope (ZEISS, Germany). Dye-positive cells were counted in a total of 18 fields per group (6 wells per group, 3 fields per well).

Western blot analysis

The cells were lysed using ice-cold Radio-Immunoprecipitation Assay (RIPA) buffer (Beyotime, P0013B). The extracts were separated on 12% SDS-PAGE, transferred to nitrocellulose membrane. The membrane were incubated with primary antibodies against GSDMD (Abcam, ab209845, 1:2000), GSDME (Abcam, ab215191, 1:2000), caspase-1 (Abcam, ab179515, 1:1000), caspase-11 (Abcam, ab22684, 1:1000), β-actin (Abcam, ab115777, 1:3000) at 4°C overnight. The membranes were then incubated with an HRP-conjugated secondary antibody for 1 h at room temperature. The epitopes were visualized using an ECL western blot detection kit (Millipore, USA).

Immunofluorescence (IF) analysis

The cells were cultured in confocal dish. Then, the cells were fixed with 4% paraformaldehyde for 30 min, permeabilized for 10 min in 0.3%Triton X-100 and blocked using 5% BSA for 1h. The cells were incubated with primary antibodies against caspase-1 (Abcam, ab179515, 1:200) or GSDMD (Abcam, ab209845, 1:200) at 4 °C overnight. The cells were washed 3times for 10min each with PBST, and then the secondary anti-Rabbit Alexa Fluor-488-conjugated antibody (Zsbio, 1:300) was added for 1 h at room temperature on the dark. Nuclear were stained with 4’, 6-diamidino-2-phenylindole (DAPI). The images were taken with ZEISS confocal microscopy system and fluorescence intensity analysis was performed with ImageJ software.

Enzyme linked immunosorbent assay (ELISA)

The levels of the inflammatory cytokines IL-1β, IL-18 and the Lactate dehydrogenase (LDH), an indicator for cell injury/death, were measured in the cell supernatants by ELISA according to the manufacturer's instructions (eBioscience, Thermo Fisher).

Cell viability

The cell viability was assessed using MTT assay Kit (Promega, USA) according to manufacturer's instructions. Approximate 4.0 $\times 10^4$ cells were plated in 96-well plates overnight. The cells were collected at various time points after carrying out OGD/R. Ten microlitre MTT solution was added to 100 uL of culture medium in each well and incubated for 4 hours at 37℃. Then the solution was removed and 100 uL of DMSO was added to each well. After mixed by oscillation 10 minutes, the optical density was measured at 570 nm by using the enzyme standard instrument. The normal cultured cells were as the control.

Inhibition of caspase-1 and GSDMD

According to the results of our preliminary experiments (supplemental Fig. 1-3), caspase-1 inhibitor AC-YVAD-CMK at 10 uM、chemical inhibitor of GSDMD Necrosulfonamide (NSA) [24] at 20uM, and a siRNA of GSDMD （siGSDMD fragment 829）was selected for their optimal inhibition effect. The peak time point of pyroptosis was subjected to the following inhibition experiments. AC-YVAD-CMK (Sigma-Aldrich, Darmstadt, Germany) or NSA (MedChemExpress, USA) dissolved in dimethylsulphoxide (DMSO) was added to the culture medium 4 hours before OGD treatment. siGSDMD-829 was transfected 48h before OGD/R, and siGSDMD-NC was transfected as the control. RNA oligonucleotides purchased from GenePharma (Shanghai, China) were transfected into cells using lipofectamine RNAiMax (Invitrogen, USA) according to the manufacturer instructions. Then, samples at the peak time point of cell pyroptosis were collected for subsequent experiments.

Transwell co-culture system for BV2 and HT22 cells

The transwell co-culture system was designed as previous reported [25]. To observe the effect of HT22 cells on BV2 cells after OGD/R, the upper layer was plated with HT22 cells and BV2 cells were cultured on the bottom well of the chamber. HT22 cells were treated with OGD/R, with or without pretreatment of AC-YVAD-CMK or NSA or siGSDMD-829 before OGD/R (as described previously). Similarly, in order to observe the effect of BV2 cells on HT22 cells after OGD/R, the BV2 cells were seeded on the upper layer, treated with OGD/R with or without pretreatment of AC-YVAD-CMK or NSA or siGSDMD-829 before OGD/R, and HT22 cells were plated on the bottom layer of the chamber. The semi-permeable membrane allows sharing of culture medium and its components between cells grown in the upper and lower chambers of the same transwell. The selection of time points for samples harvested from the lower chamber was in accordance with the peak time point of the corresponding cell pyroptosis observed in the foregoing experiment. The samples of the lower cells were collected for subsequent experiments.

Statistical Analysis

Statistical analysis was performed using the GraphPad Prism Software. The ImageJ software was used to analyze the optical density of the western blot results and to calculate the number of pyroptotic cells. Values were presented as the means ± SEM with the homogeneity of variance. The Student t-test was used for the difference between the two groups of independent data. The comparison between multiple groups of samples was performed by one-way ANOVA. $P<0.05$ indicated statistical difference, and each experiment was repeated three times.

Results

BV2 and HT22 cells underwent cell pyroptosis after OGD/R

The experimental results of the BV2 cell pyroptosis after OGD/R were as followed. The dye uptake method showed the highest proportion of pyroptotic cells appeared at 12h after OGD/R (Fig. 2a-2b). Western blot results demonstrated that GSDMD-N and cleaved-caspase-1 expression increased at 12h after OGD/R, but the levels of GSDME-N and cleaved-caspase-11 were not upregulated in all time points after OGD/R (Fig. 2c-2k). Immunofluorescence results showed that caspase-1 and GSDMD expression increased at 12h after OGD/R (Fig. 2l-2o). In addition, IL-1β, IL-18 and LDH in cell supernatant were significantly increased (Fig. 2p-2r) and the cell viability was significantly decreased at 6h, 12h(most obvious) and 24h after OGD/R (Fig. 2s).

Similar trend in changes of pyroptosis markers was also observed in neuronal cell line HT22 after OGD/R, which reached the peak at 6h time point after OGD/R, a phenomenon that is 6h earlier than BV2 cells (Fig. 3).

Inhibition of caspase-1 alleviated BV2 and HT22 cell pyroptosis and GSDMD activation after OGD/R

Based on the above experimental results, BV2 cells at 12h and HT22 cells at 6h after OGD/R were used to observe the inhibitory effects of caspase-1 and GSDMD.

After pretreatment of AC-YVAD-CMK, a caspase-1 inhibitor, the proportion of pyroptotic BV2 and HT22 cells was significantly decreased (Fig. 4a-4b, 4i-4j). AC-YVAD-CMK reduced caspase-1 cleavage and activation (supplemental Fig. 1), and down-regulated the processing of GSDMD-N in cells after OGD/R (Fig. 4c-4e, 4k-4m). Production of IL-1β, IL-18, and LDH in cell supernatant was also significantly decreased in cells pre-treated with AC-YVAD-CMK (Fig. 4f-4h, 4n-4p). Notably, the levels of IL-1β, IL-18 and LDH in HT22 cells were less than that in BV2 cells.

Inhibition of GSDMD alleviated BV2 and HT22 cell pyroptosis after OGD/R

After pretreatment of NSA, an inhibitor of GSDMD, or transfected with siGSDMD-829, which knocked down cellular GSDMD expression (Fig. 6c-6e, 6k-6m), the proportion of pyroptotic BV2 and HT22 cells was significantly decreased (Fig. 5a-5b, 5i-5j; 6a-6b, 6i-6j). NSA down-regulated the processing of

GSDMD-N in cells after OGD/R (Fig. 5c-5e, 5k-5m). Production of IL-1β, IL-18, and LDH in cell supernatant was also significantly decreased in cells pre-treated with NSA or siGSDMD-829 (Fig 5f-5h, 5n-5p; 6f-6h, 6n-6p). Notably, the levels of IL-1β, IL-18 and LDH in HT22 cells were less than that in BV2 cells.

HT22 and BV2 cells undergoing OGD/R aggravated pyroptosis of adjacent non-OGD/R-treated cells

Using the transwell co-culture model, HT22 cells were seeded in the upper layer of the chamber and underwent OGD/R treatment for 6h, then HT22 cells were co-cultured with BV2 cells for additional 12h. Greater proportion of pyroptotic cells (Fig. 7a-7b), increased GSDMD-N expression (Fig. 7c-7e), higher level of IL-1β, IL-18 and LDH (Fig. 7f-7h) and decreased cell viability (Fig. 7i) were observed in the co-cultured BV2 cells as compared with BV2 cells cultured alone and were treated by OGD/R for 12h.

Similar results were found in the transwell co-culturing experiments, in which BV2 cells were seeded in the upper layer and underwent OGD/R for 12h, then co-cultured with HT22 cells in the lower layer for additional 6h. Compared with HT22 cells treated by OGD/R for 6h, the HT22 cells co-cultured with OGD/R-treated BV2 cells showed greater proportion of pyroptotic cells (Fig. 7j-7k), increased GSDMD-N expression (Fig. 7l-7n), higher level of IL-1β, IL-18 and LDH (Fig. 7o-7q) and decreased cell viability (Fig. 7r). However, levels of secreted IL-1β, IL-18 and LDH found in HT22 culture medium could be contributed from co-cultured BV2 cells and therefore may not necessarily reflect the changes of HT22.

Inhibition of caspase-1 in HT22 cells before OGD/R alleviated pyroptosis of adjacent BV2 cells, and vice versa

Using the transwell model, HT22 cells were pretreated with AC-YVAD-CMK before OGD/R, followed by co-culturing with BV2 cells seeded in the lower layer of the chamber for additional 12h. Reduction in pyroptotic cells (Fig. 8a-8b), decreased GSDMD-N expression (Fig. 8c-8e), lowered levels of IL-1β, IL-18 and LDH (Fig. 8f-8h) were observed in the co-cultured BV2 cells as compared with BV2 cells that were co-cultured with OGD/R-treated HT22 without AC-YVAD-CMK pretreatment.

Similar phenomenon was found in the transwell co-culture model in which BV2 cells were pretreated with AC-YVAD-CMK before OGD/R, followed by co-culturing with HT22 cells in the same chamber for additional 6h. Compared with HT22 cells in the transwell co-culture model, in which BV2 cells were not pretreated with AC-YVAD-CMK before OGD/R, the lower HT22 cells showed fewer proportion of pyroptotic cells (Fig. 8i-8j), decreased GSDMD-N production (Fig. 8k-8m) and lowered level of IL-1β, IL-18 and LDH in the culture medium (Fig. 8n-8p). Similarly, levels of secreted IL-1β, IL-18 and LDH found in HT22 culture medium could be contributed from co-cultured BV2 cells and therefore may not necessarily reflect the changes of HT22.

Inhibition of GSDMD in HT22 cells before OGD/R alleviated pyroptosis of adjacent BV2 cells, and vice versa

Using the transwell model, HT22 cells were pretreated with NSA or siGSDMD-829 before OGD/R, followed by co-culturing with BV2 cells seeded in the lower layer of the chamber for additional 12h. Reduction in

pyroptotic cells (Fig. 9a-9b,10a-10b), decreased GSDMD-N expression (Fig. 9c-9e,10c-10e), lowered levels of IL-1β, IL-18 and LDH (Fig. 9f-9h, 10f-10h) were observed in the co-cultured BV2 cells as compared with BV2 cells that were co-cultured with OGD/R-treated HT22 without AC-YVAD-CMK pretreatment.

Similar phenomenon was found in the transwell co-culture model in which BV2 cells were pretreated with NSA or siGSDMD-829 before OGD/R, followed by co-culturing with HT22 cells in the same chamber for additional 6h. Compared with HT22 cells in the transwell co-culture model, in which BV2 cells were not pretreated with NSA or siGSDMD-829 before OGD/R, the lower HT22 cells showed fewer proportion of pyroptotic cells (Fig. 9i-9j, 10i-10j), decreased GSDMD-N production (Fig. 9k-9m, 10k-10m) and lowered level of IL-1β, IL-18 and LDH in the culture medium (Fig. 9n-9p, 10n-10p). Similarly, levels of secreted IL-1β, IL-18 and LDH found in HT22 culture medium could be contributed from co-cultured BV2 cells and therefore may not necessarily reflect the changes of HT22.

Discussion

To our knowledge,it is first study to comprehensively explore the mechanisms and interactions of microglial and neuronal cell pyroptosis after I/R. The results here showed that in the simulated I/R environment in vitro (the OGD/R model), both BV2 and HT22 cells underwent pyroptosis, and the onset of pyroptosis of HT22 cells was 6 h earlier than that of BV2 cells. Our data also showed no significant changes in caspase-11 and GSDME expression in BV2 and HT22 cells after OGD/R. Inhibition of caspase-1 or GSDMD alleviated BV2 and HT22 cell pyroptosis after OGD/R, and GSDMD activation was suppressed by caspase-1 inhibitor. HT22 or BV2 cells undergoing OGD/R aggravated pyroptosis of adjacent BV2 or HT22 cells, respectively, which was relieved by inhibition of caspase-1 or GSDMD.

A number of studies have identified that the activation of the Gasdermin family proteins is the biological marker for pyroptosis [26–29]. Few studies have observed that GSDMD was activated in primary cultured cortical neurons or microglia or BV2 cells undergoing OGD or OGD/R [21–23], but the time point of GSDMD activation in these studies is different from that in our study, which may be due to the difference in cell type or culture condition. Our study observed the activation of GSDMD in BV2 and HT22 cells after OGD/R. Moreover, for the first time the dye uptake method was used in the brain injury model of in vitro to prove the occurrence of pyroptosis. The results showed that HT22 cells developed cell pyroptosis earlier than BV2 cells, which may help explain the cell type-specific susceptibility in vivo because neurons are more vulnerable to ischemia-induced injury than microglia [30–32]. In our study, we also found no changes in GSDME activation in both neuronal cells and microglia after OGD/R.

The mechanisms of BV2 and HT22 cell pyroptosis after OGD/R were further explored in our study. The results demonstrated that inhibition of caspase-1 could alleviate GSDMD activation, and inhibition of caspase-1 or GSDMD could reduce the level of IL-1β, IL-18 and LDH in both cell types after OGD/R, which is similar to the results reported by Poh et al [21] and Tang et al [23]. However,caspase-11 and GSDME activation in BV2 and HT22 cells following OGD/R were not found in our study. Fann et al [30] reported that caspase-11 expression was increased in primary cultured cortical neurons after OGD/R, which is

different from our results. As described above, the difference may be due to cell type or culture condition. Based on our findings, we speculate that activation of the canonical inflammasome pathway(caspase-1/GSDMD) is crucial for cell pyroptosis but caspase-3/GSDME pathway may not be involved in pyroptotic cell death following brain I/R. Whether the non-canonical inflammasome pathway (caspase-11/GSDMD) play a role in cell pyroptosis following brain I/R remains to be determined. In addition，in our study, for the first time we showed that necrosulfonamide (NSA) was able to inhibit GSDMD-induced pyroptosis following I/R. The results showed here strongly suggest that NSA could be an effective suppressor for the activation of GSDMD induced by OGD/R. Further investigation on the protective effect of NSA in I/R animal model is warranted.

After cell pyroptosis, the release of cellular contents, including damage associated molecular patterns (DAMPs), and their binding to pattern recognition receptors (PRRs) on the adjacent cells result in inflammatory propagation [34, 35]. In addition, studies of]inflammatory diseases have demonstrated that inflammasome components released from the pyroptotic cells could re-assemble into functional complexes or could be engulfed by neighboring phagocytic cells to further activate caspase-1, which helps amplify and prolong the inflammatory response [36, 37]. However,it is not clear yet whether the cell pyroptosis induced by I/R propagate inflammation. In this study, by using the transwell co-culture system, we observed that HT22 or BV2 cells undergoing OGD/R can not only produce pyroptosis phenotype, but also induce pyroptotic death of their neighboring BV2 or HT22 cells with more severe cell death phenotype than that of those cells treated with OGD/R alone. After inhibition of caspase-1 or GSDMD of HT22 or BV2 cells undergoing OGD/R, pyroptotic death of the neighboring BV2 or HT22 cells was alleviated. These results imply that the sequential induction of microglial and neuronal pyroptosis after cerebral I/R may result in an amplifying cascade of inflammatory response and prolonged tissue damage.

Conclusion

In summary, our study demonstrated that microglia and neurons underwent pyroptosis during mimic I/R injury in vitro,which was attributed to the activation of caspase-1/GSDMD pathway without the involvement of other known pyroptosis pathways. Moreover, the cell pyroptosis occurred in neurons and microglia after I/R could trigger pyroptosis in other adjacent but non-OGD/R cells. Our findings suggest that caspase-1 and GSDMD are important therapeutic targets for cerebral I/R-induced tissue damage and inflammation. Furthermore, NSA, a direct chemical inhibitor of GSDMD, may be a potential drug candidate to treat cerebral I/R-induced injury, and its further investigation is warranted.

Abbreviations

DAMPs: damage associated molecular patterns; ELISA: Enzyme linked immunosorbent assay; GSDMD : Gasdermin D; GSDME : Gasdermin E; GSDMD-N : the N-terminal domain of GSDMD; I/R: ischemia/reperfusion; NSA: Necrosulfonamide; OGD/R : oxygen-glucose deprivation/reoxygenation.

Declarations

Ethics Approval and consent to participate

Not applicable.

Acknowledgements

The authors would thank Research Center of Medicine, Sun Yat-Sen Memorial Hospital for providing necessary infrastructure support to accomplish this work.

Funding

This research was supported by the Natural Science Foundation of Guangdong Province, China (2017A030313869) and the Science and Technology Project of Guangzhou City, China (201607010325), the National Natural Science Foundation of China (No. 81171103) and Guangdong Science and Technology Department (2017B030314026).

Authors' contributions

ZFD, KP, YDW and WJL, conceived and designed the experiments. ZFD and QXP performed the experiments and analyzed the data. YDW and WJL contributed reagents/materials/analysis tools. ZFD wrote the first draft of the paper. WJL and YDW contributed to the writing of the paper. All authors read and approved the final manuscript.

Conflict of Interest

The authors declare that there are no conflicts of interest.

Availability of data and materials

The datasets used and analyzed during the current study are available from

the corresponding author on reasonable request.

Consent for publication

Not applicable.

References

1. Hu X, De Silva TM, Chen J, Faraci FM. Cerebral Vascular Disease and Neurovascular Injury in Ischemic Stroke. Circ Res.2017;120:449-471.
2. Powers WJ, Rabinstein AA, Ackerson T *et al.* 2018 Guidelines for the Early Management of Patients With Acute Ischemic Stroke: A Guideline for Healthcare Professionals From the American Heart Association/American Stroke Association. Stroke.2018;49:e46-e110.
3. Alberts MJ. Stroke Treatment With Intravenous Tissue-Type Plasminogen Activator: More Proof That Time Is Brain. Circulation.2017;135:140-142.
4. Mizuma A, Yenari MA. Anti-Inflammatory Targets for the Treatment of Reperfusion Injury in Stroke. Front Neurol.2017;8:467.
5. Hossmann KA. The two pathophysiologies of focal brain ischemia: implications for translational stroke research. J Cereb Blood Flow Metab.2012;32:1310-1316.
6. Voet S, Srinivasan S, Lamkanfi M, van Loo G. Inflammasomes in neuroinflammatory and neurodegenerative diseases. EMBO Mol Med.2019;11.
7. Walsh JG, Muruve DA, Power C. Inflammasomes in the CNS. Nat Rev Neurosci.2014;15:84-97.
8. Lampron A, Elali A, Rivest S. Innate immunity in the CNS: redefining the relationship between the CNS and Its environment. Neuron.2013;78:214-232.
9. Liddelow SA, Guttenplan KA, Clarke LE *et al.* Neurotoxic reactive astrocytes are induced by activated microglia. Nature.2017;541:481-487.
10. Bergsbaken T, Fink SL, Cookson BT. Pyroptosis: host cell death and inflammation. Nat Rev Microbiol.2009;7:99-109.
11. Dong Z, Pan K, Pan J, Peng Q, Wang Y. The Possibility and Molecular Mechanisms of Cell Pyroptosis After Cerebral Ischemia. Neurosci Bull.2018;34:1131-1136.
12. Adamczak SE, de Rivero Vaccari JP, Dale G *et al.* Pyroptotic neuronal cell death mediated by the AIM2 inflammasome. J Cereb Blood Flow Metab.2014;34:621-629.
13. Galluzzi L, Vitale I, Abrams JM *et al.* Molecular definitions of cell death subroutines: recommendations of the Nomenclature Committee on Cell Death 2012. Cell Death Differ.2012;19:107-120.
14. Miao EA, Rajan JV, Aderem A. Caspase-1-induced pyroptotic cell death. Immunol Rev.2011;243:206-214.

15. Shi J, Zhao Y, Wang K *et al.* Cleavage of GSDMD by inflammatory caspases determines pyroptotic cell death. Nature.2015;526:660-665.
16. Kayagaki N, Stowe IB, Lee BL *et al.* Caspase-11 cleaves gasdermin D for non-canonical inflammasome signalling. Nature.2015;526:666-671.
17. He WT, Wan H, Hu L *et al.* Gasdermin D is an executor of pyroptosis and required for interleukin-1beta secretion. Cell Res.2015;25:1285-1298.
18. Rogers C, Fernandes-Alnemri T, Mayes L *et al.* Cleavage of DFNA5 by caspase-3 during apoptosis mediates progression to secondary necrotic/pyroptotic cell death. Nat Commun.2017;8:14128.
19. Wang Y, Gao W, Shi X *et al.* Chemotherapy drugs induce pyroptosis through caspase-3 cleavage of a gasdermin. Nature.2017;547:99-103.
20. Wang Y, Yin B, Li D *et al.* GSDME mediates caspase-3-dependent pyroptosis in gastric cancer. Biochem Biophys Res Commun.2018;495:1418-1425.
21. Poh L, Kang SW, Baik SH *et al.* Evidence that NLRC4 inflammasome mediates apoptotic and pyroptotic microglial death following ischemic stroke. Brain Behav Immun.2019;75:34-47.
22. Zhang D, Qian J, Zhang P *et al.* Gasdermin D serves as a key executioner of pyroptosis in experimental cerebral ischemia and reperfusion model both in vivo and in vitro. J Neurosci Res.2019;97:645-660.
23. Tang M, Li X, Liu P *et al.* Bradykinin B2 receptors play a neuroprotective role in Hypoxia/reoxygenation injury related to pyroptosis pathway. Curr Neurovasc Res.2018;15:138-144.
24. Rathkey JK, Zhao J, Liu Z *et al.* Chemical disruption of the pyroptotic pore-forming protein gasdermin D inhibits inflammatory cell death and sepsis. Sci Immunol.2018;3.
25. Kaushal V, Schlichter LC. Mechanisms of microglia-mediated neurotoxicity in a new model of the stroke penumbra. J Neurosci.2008;28:2221-2230.
26. Ding J, Wang K, Liu W *et al.* Pore-forming activity and structural autoinhibition of the gasdermin family. Nature.2016;535:111-116.
27. Chen X, He WT, Hu L *et al.* Pyroptosis is driven by non-selective gasdermin-D pore and its morphology is different from MLKL channel-mediated necroptosis. Cell Res.2016;26:1007-1020.
28. Liu X, Zhang Z, Ruan J *et al.* Inflammasome-activated gasdermin D causes pyroptosis by forming membrane pores. Nature.2016;535:153-158.
29. Sborgi L, Ruhl S, Mulvihill E *et al.* GSDMD membrane pore formation constitutes the mechanism of pyroptotic cell death. EMBO J.2016;35:1766-1778.
30. Brown GC, Vilalta A. How microglia kill neurons. Brain Res.2015;1628:288-297.
31. von Bernhardi R, Eugenin-von Bernhardi J, Flores B, Eugenin Leon J. Glial Cells and Integrity of the Nervous System. Adv Exp Med Biol.2016;949:1-24.
32. Vannucci SJ, Maher F, Simpson IA. Glucose transporter proteins in brain: delivery of glucose to neurons and glia. Glia.1997;21:2-21.

33. Fann DY, Lee SY, Manzanero S *et al.* Intravenous immunoglobulin suppresses NLRP1 and NLRP3 inflammasome-mediated neuronal death in ischemic stroke. Cell Death Dis.2013;4:e790.
34. Kono H, Kimura Y, Latz E. Inflammasome activation in response to dead cells and their metabolites. Curr Opin Immunol.2014;30:91-98.
35. Kono H, Onda A, Yanagida T. Molecular determinants of sterile inflammation. Curr Opin Immunol.2014;26:147-156.
36. Franklin BS, Bossaller L, De Nardo D *et al.* The adaptor ASC has extracellular and 'prionoid' activities that propagate inflammation. Nat Immunol.2014;15:727-737.
37. Baroja-Mazo A, Martin-Sanchez F, Gomez AI *et al.* The NLRP3 inflammasome is released as a particulate danger signal that amplifies the inflammatory response. Nat Immunol.2014;15:738-748.

Table

Table 1 The sequences of GSDMD siRNA and Negative control

Gene	sequence（5'-3'）
Gsdmd-Mus-312	F: CAUGUGUCAACCUGUCAAUTT
	R: AUUGACAGGUUGACACAUGTT
Gsdmd-Mus-829	F: GGAUAUCCUUCUCGUCUCATT
	R: UGAGACGAGAAGGAUAUCCTT
Gsdmd-Mus-1477	F: GCUAGAAGAAUGUGGCCUATT
	R: UAGGCCACAUUCUUCUAGCTT
Gsdmd-Mus-1582	F: GUCAAGUCUAGGCCAGAAATT
	R: UUUCUGGCCUAGACUUGACTT
Negative control	F: UUCUCCGAACGUGUCACGUTT
	R: ACGUGACACGUUCGGAGAATT

Supplemental Figures

Supplemental Fig.1 Appropriate inhibitory concentration of caspase-1 was screened by immunoblot method. a-c. Representative immunoblot and its quantification of caspase-1 and cleaved-caspase-1. Cleaved-caspase-1 expression is lowest at 10uM YVAD. β-actin was used as a loading control. All data were represented as mean ± SEM. n=3, *P<0.05 compared with DMSO group. N.S means nonsignificant difference.

Supplemental Fig.2 Appropriate inhibitory concentration of necrosulfonamide (NSA) was screened by immunoblot method. a-c. Representative immunoblot and its quantification of GSDMD-F and GSDMD-N. GSDMD-N expression is lowest at 20uM YVAD. β-actin was used as a loading control. All data were represented as mean ± SEM. n=3, *P<0.05 compared with DMSO group. N.S means nonsignificant difference.

Supplemental Fig.3 Appropriate siRNA fragments of GSDMD was screened by immunoblot method. a-b. Representative immunoblot and its quantification of GSDMD. GSDMD expression was lowest when transfected with siRNA-829. β-actin was used as a loading control. All data were represented as mean ± SEM. n=3, *P<0.05 compared with control. N.S means nonsignificant difference.

Figures

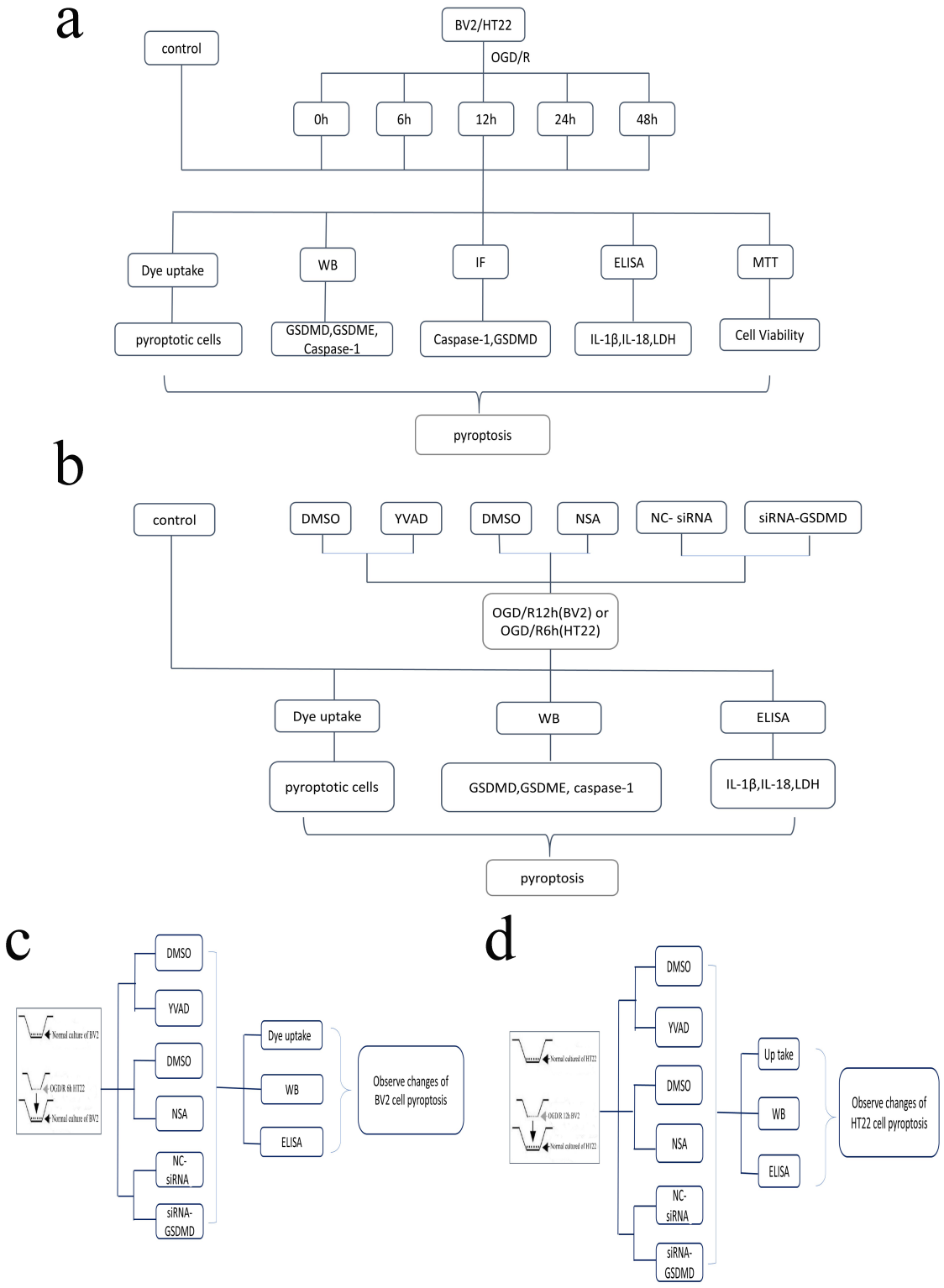

Figure 1

Experimental design. a. Flow chart of detection of BV2 and HT22 cell pyroptosis，pyroptosis-related proteins and cell viability after OGD/R. b. Flow chart of demonstrating the effect of inhibition of caspase-1 or GSDMD on BV2 and HT22 cell pyroptosis following OGD/R. c and d. Flow chart of exploring the interaction of BV2 and HT22 cell pyroptosis after OGD/R by the transwell co-culture system. OGD/R， oxygen-glucose deprivation/reoxygenation

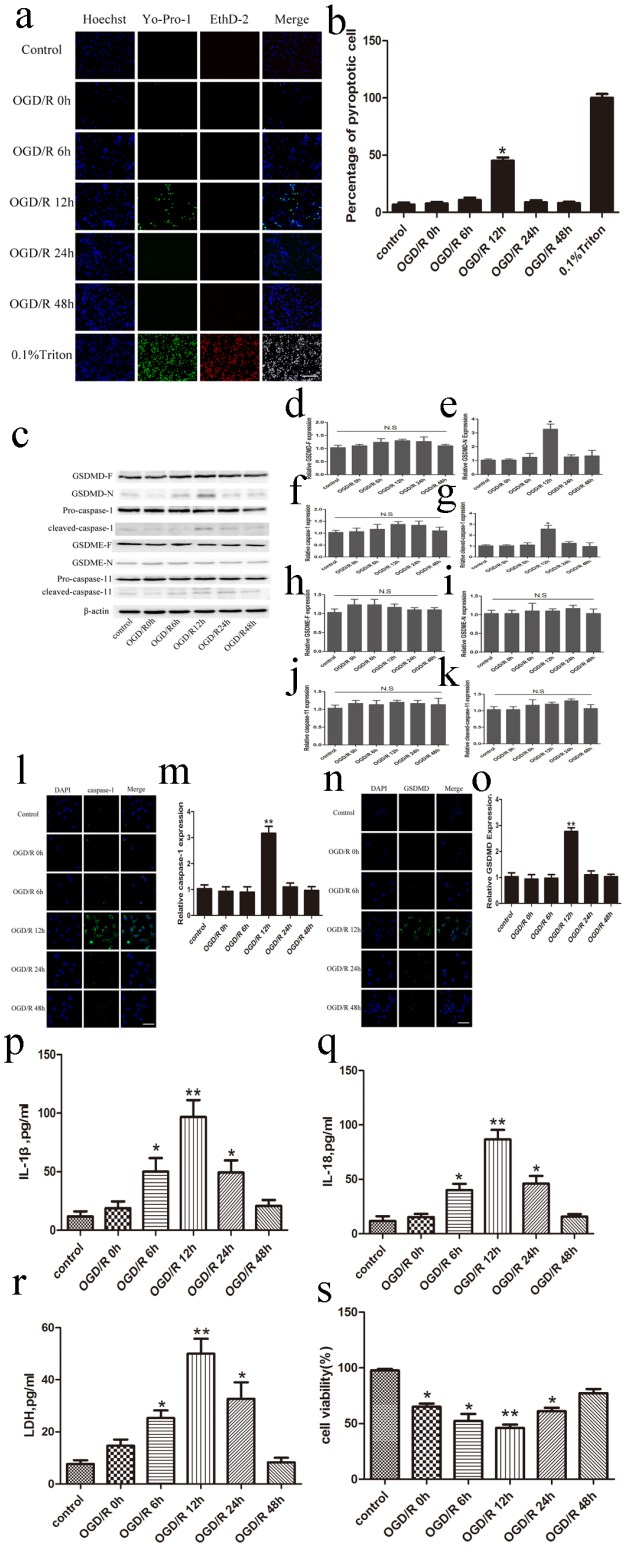

Figure 2

BV2 cells underwent cell pyroptosis after OGD/R. a and b. Representative immunofluorescence staining of BV2 cells by dye uptake method (a) and histogram of the percentage of pyroptotic BV2 cells(b). The highest proportion of pyroptotic BV2 cells appeared at 12h after OGD/R. 0.1% Triton X-100 was used as a positive control. Magnification, ×100. Scale bar, 100um. c-k. Representative immunoblot and quantification results of pyroptosis-related proteins in BV2 cells at the indicated time points during

OGD/R. GSDMD-N and cleaved-caspase-1 expression increased at 12h after OGD/R. β-actin was used as a loading control. l-o. Representative immunofluorescence staining (l, n) and histogram of the relative expression m, o of caspase-1 and GSDMD in BV2 cells. Caspase-1 and GSDMD expression increased at 12h after OGD/R. Magnification, ×600. Scale bar, 200um. p-r. ELISA results showed that the highest level of IL-1β, IL-18 and LDH in cell supernatant of BV2 cells appeared at 12h after OGD/R. s. The cell viability of BV2 cells was detected by MTT assay kit. The minimum cell proliferative ability appeared at 12h after OGD/R. All data were represented as mean ± SEM. n=3, *P<0.05, **P<0.01 compared with control. N.S, no significant difference.

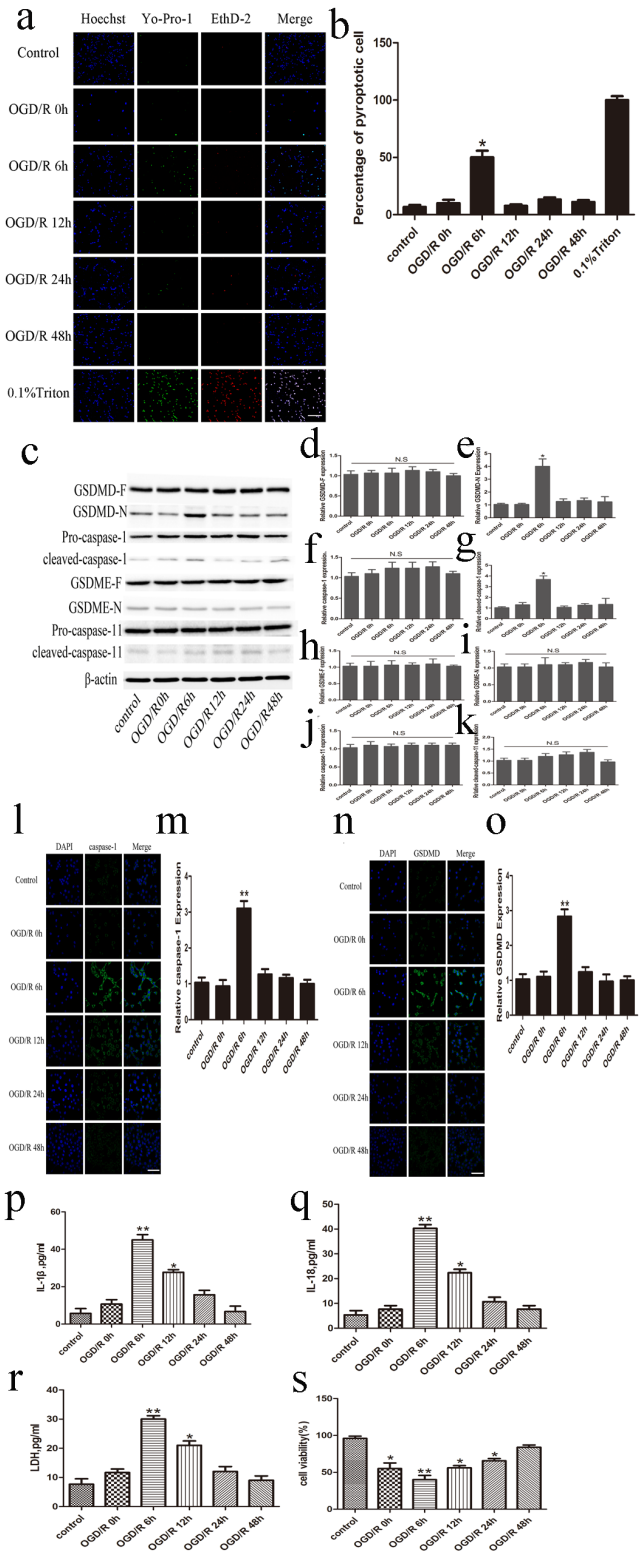

Figure 3

HT22 cells underwent cell pyroptosis after OGD/R. a and b. Representative immunofluorescence staining of HT22 cells by dye uptake method (a) and histogram of the percentage of pyroptotic HT22 cells (b). The highest proportion of pyroptotic HT22 cells appeared at 6h after OGD/R. 0.1% Triton X-100 was used as a positive control. Magnification, ×100. Scale bar, 100um. c-k. Representative immunoblot and its quantification of pyroptosis-related proteins in HT22 cells at the indicated time points during OGD/R.

GSDMD-N and cleaved-caspase-1 expression increased at 6h after OGD/R. β-actin was used as a loading control. l-o. Representative immunofluorescence staining (l, n) and histogram of the relative expression m, o of caspase-1 and GSDMD in HT22 cells. Caspase-1 and GSDMD expression increased at 6h after OGD/R Magnification, ×600. Scale bar, 200um. p-r. ELISA results showed that the highest level of IL-1β, IL-18 and LDH in cell supernatant of HT22 cells appeared at 6h after OGD/R. s. The cell viability of HT22 cells was detected by MTT assay Kit. The minimum cell proliferative ability appeared at 6h after OGD/R. All data were represented as mean ± SEM. n=3, *P<0.05, **P<0.01. N.S, no significant difference.

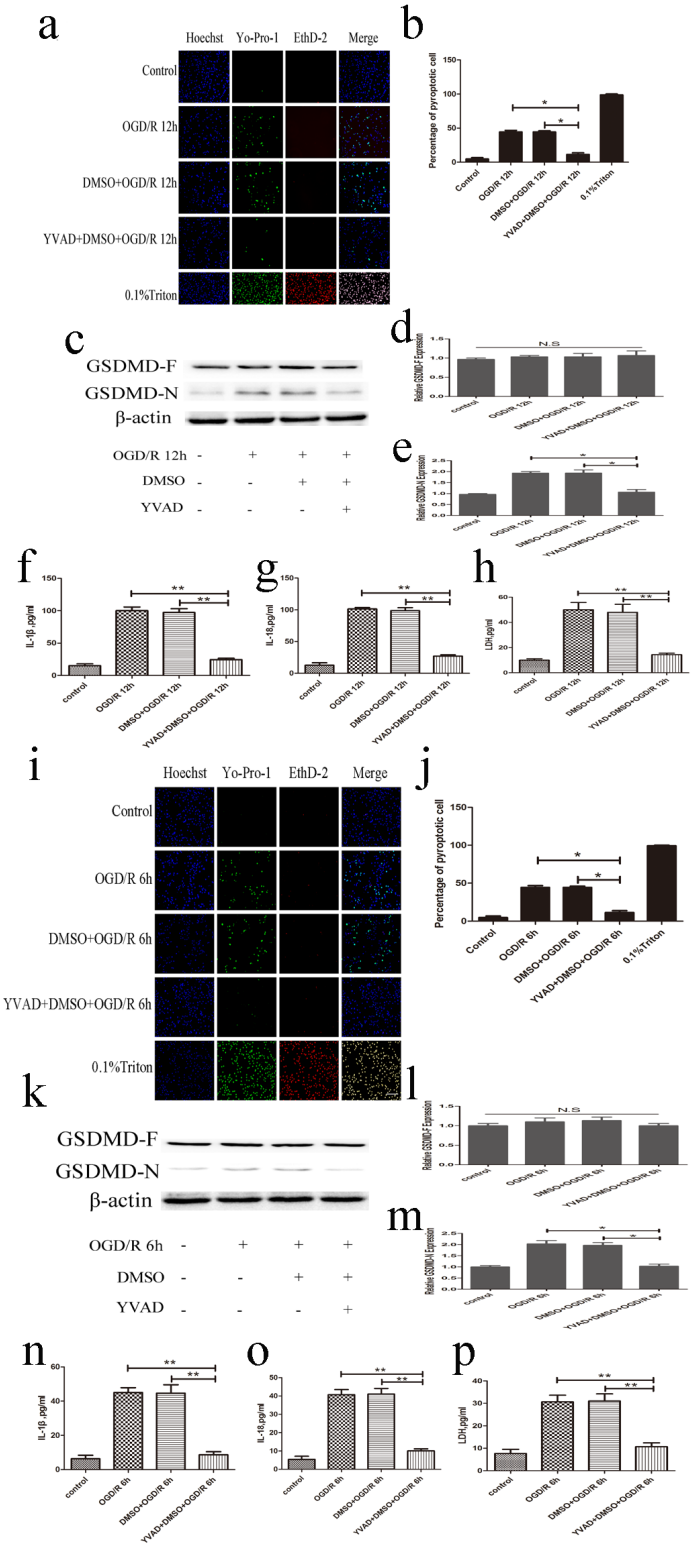

Figure 4

Inhibition of caspase-1 alleviated BV2 and HT22 cell pyroptosis and GSDMD activation after OGD/R. a and b. Representative immunofluorescence staining of BV2 cells by dye uptake method (a) and histogram of the percentage of pyroptotic BV2 cells (b). After BV2 cells were pretreated with AC-YVAD-CMK (YVAD), a specific inhibitor of caspase-1, the proportion of pyroptotic BV2 cells was decreased at 12h after OGD/R. 0.1% Triton X-100 was used as a positive control. Magnification, ×100. Scale bar, 100um. c-e. Representative immunoblot and its quantification of GSDMD protein in BV2 cell. After BV2 cells were pretreated with YVAD, the GSDMD-N expression was downregulated at 12h after OGD/R. β-actin was used as a loading control. f-h. ELISA results showed that the level of IL-1β, IL-18 and LDH in cell supernatant of BV2 cells pretreated with YVAD was significantly decreased at 12h after OGD/R. i -j. Representative immunofluorescence staining of HT22 cells by dye uptake method (i) and histogram of the percentage of pyroptotic HT22 cells (j). After HT22 cells were pretreated with YVAD, the proportion of pyroptotic HT22 cells was decreased at 6h after OGD/R. 0.1% Triton X-100 was used as a positive control. Magnification, ×100. Scale bar, 100um. k-m. Representative immunoblot and its quantification of GSDMD protein in HT22 cell. After HT22 cells were pretreated with YVAD, the GSDMD-N expression was downregulated at 6h after OGD/R. β-actin was used as a loading control. n-p. ELISA results showed that the level of IL-1β, IL-18 and LDH in cell supernatant of HT22 cells pretreated with YVAD was significantly decreased at 6h after OGD/R. All data were represented as mean ± SEM. n=3, *P<0.05, **P<0.01 compared with the group pretreated with YVAD. N.S, no significant difference.

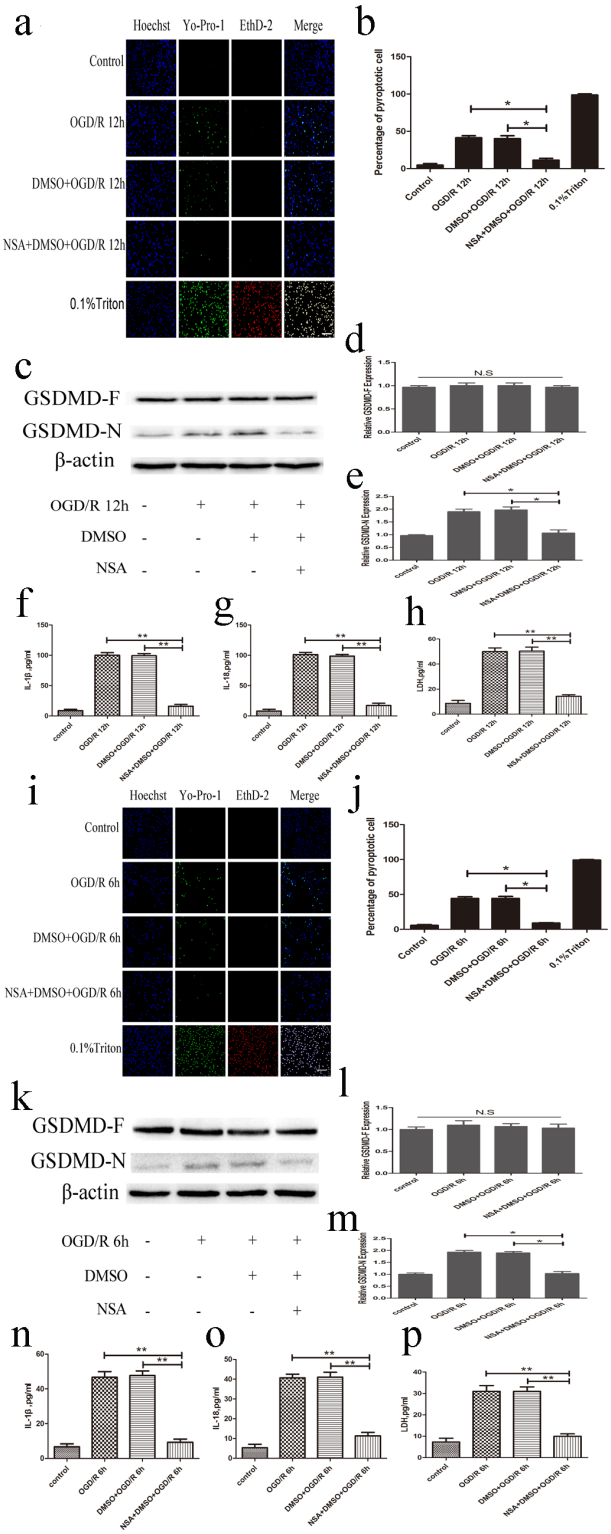

Figure 5

Inhibition of GSDMD by necrosulfonamide (NSA) alleviated BV2 and HT22 cell pyroptosis after OGD/R. a and b. Representative immunofluorescence staining of BV2 cells by dye uptake method (a) and histogram of the percentage of pyroptotic BV2 cells (b). After BV2 cells were pretreated with NSA, a chemical inhibitor of GSDMD, the proportion of pyroptotic BV2 cells was decreased at 12h after OGD/R. 0.1% Triton X-100 was used as a positive control. Magnification, ×100. Scale bar, 100um. c-e.

Representative immunoblot and its quantification of GSDMD protein in BV2 cell. After BV2 cells were pretreated with NSA, the GSDMD-N expression was downregulated at 12h after OGD/R. β-actin was used as a loading control. f-h. ELISA results showed that the level of IL-1β, IL-18 and LDH in cell supernatant of BV2 cells pretreated with NSA was significantly decreased at 12h after OGD/R. i-j. Representative immunofluorescence staining of HT22 cells by dye uptake method (i) and histogram of the percentage of pyroptotic HT22 cells (j). After HT22 cells were pretreated with NSA, the proportion of pyroptotic HT22 cells was decreased at 6h after OGD/R. 0.1% Triton X-100 was used as a positive control. Magnification, ×100. Scale bar, 100um. k-m. Representative immunoblot and its quantification of GSDMD protein in HT22 cell. After HT22 cells pretreated with NSA, the GSDMD-N expression was downregulated at 6h after OGD/R. β-actin was used as a loading control. n-p. ELISA results showed that the level of IL-1β, IL-18 and LDH in cell supernatant of HT22 cells pretreated with NSA was significantly decreased at 6h after OGD/R. All data were represented as mean ± SEM. n=3, *P<0.05, **P<0.01 compared with the group pretreated with NSA. N.S means nonsignificant difference.

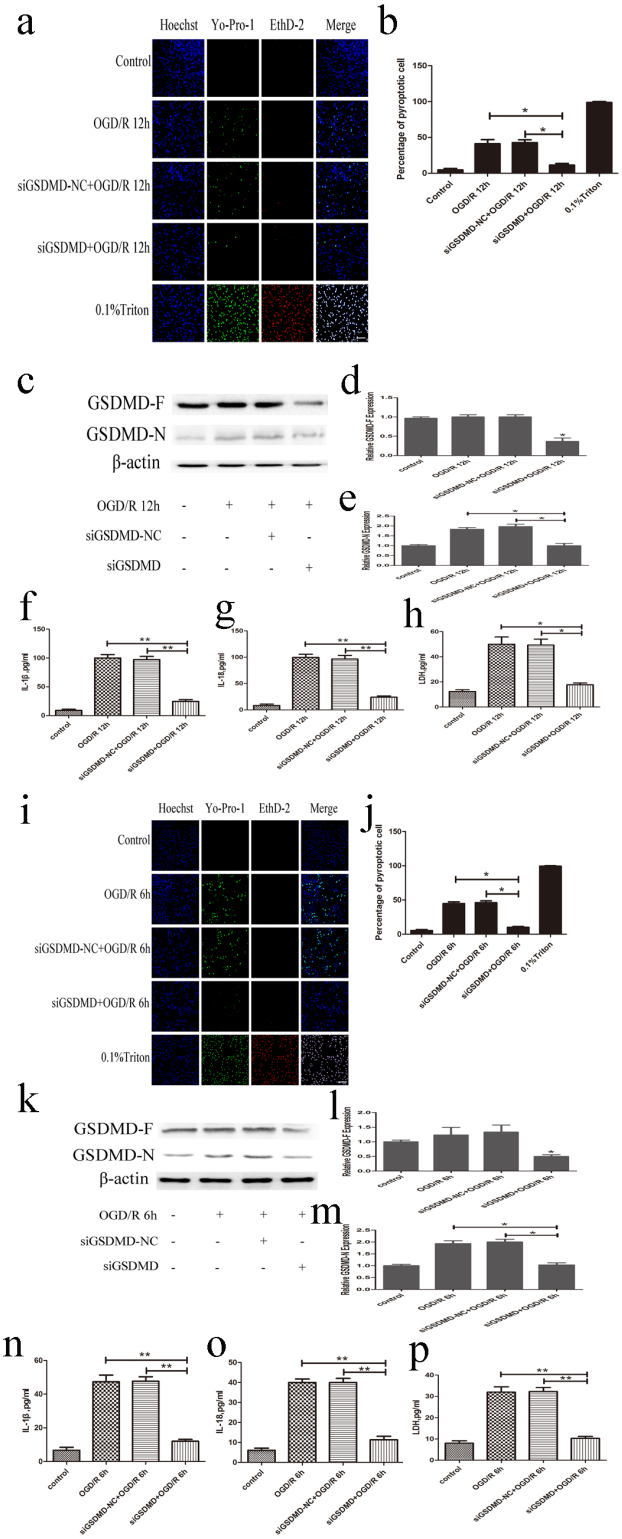

Figure 6

Knockdown GSDMD with siRNA alleviated BV2 and HT22 cell pyroptosis after OGD/R. a and b. Representative immunofluorescence staining of BV2 cells by dye uptake method (a) and histogram of the percentage of pyroptotic BV2 cells (b). After BV2 cells were pretreated with siRNA of GSDMD （siGSDMD）, the proportion of pyroptotic BV2 cells was decreased at 12h after OGD/R. 0.1% Triton X-100 was used as a positive control. Magnification, ×100. Scale bar, 100um. c-e. Representative immunoblot and its

quantification of GSDMD protein in BV2 cell. After BV2 cells were pretreated with siGSDMD, the GSDMD-N and GSDMD-F expression were downregulated at 12h after OGD/R. β-actin was used as a loading control. f-h. ELISA results showed that the level of IL-1β, IL-18 and LDH in cell supernatant of BV2 cells pretreated with siGSDMD was significantly decreased at 12h after OGD/R. i-j. Representative immunofluorescence staining of HT22 cells by dye uptake method (i) and histogram of the percentage of pyroptotic HT22 cells (j). After HT22 cells were pretreated with siGSDMD, the proportion of pyroptotic HT22 cells was decreased at 6h after OGD/R. 0.1% Triton X-100 was used as a positive control. Magnification, ×100. Scale bar, 100um. k-m. Representative immunoblot and its quantification of GSDMD protein in HT22 cell. After HT22 cells were pretreated with siGSDMD, the GSDMD-N and GSDMD-F expression were downregulated at 6h after OGD/R. β-actin was used as a loading control. n-p. ELISA results showed that the level of IL-1β, IL-18 and LDH in cell supernatant of HT22 cells pretreated with siGSDMD was significantly decreased at 6h after OGD/R. All data were represented as mean ± SEM. n=3, *P<0.05, **P<0.01 compared with the group pretreated with siGSDMD.

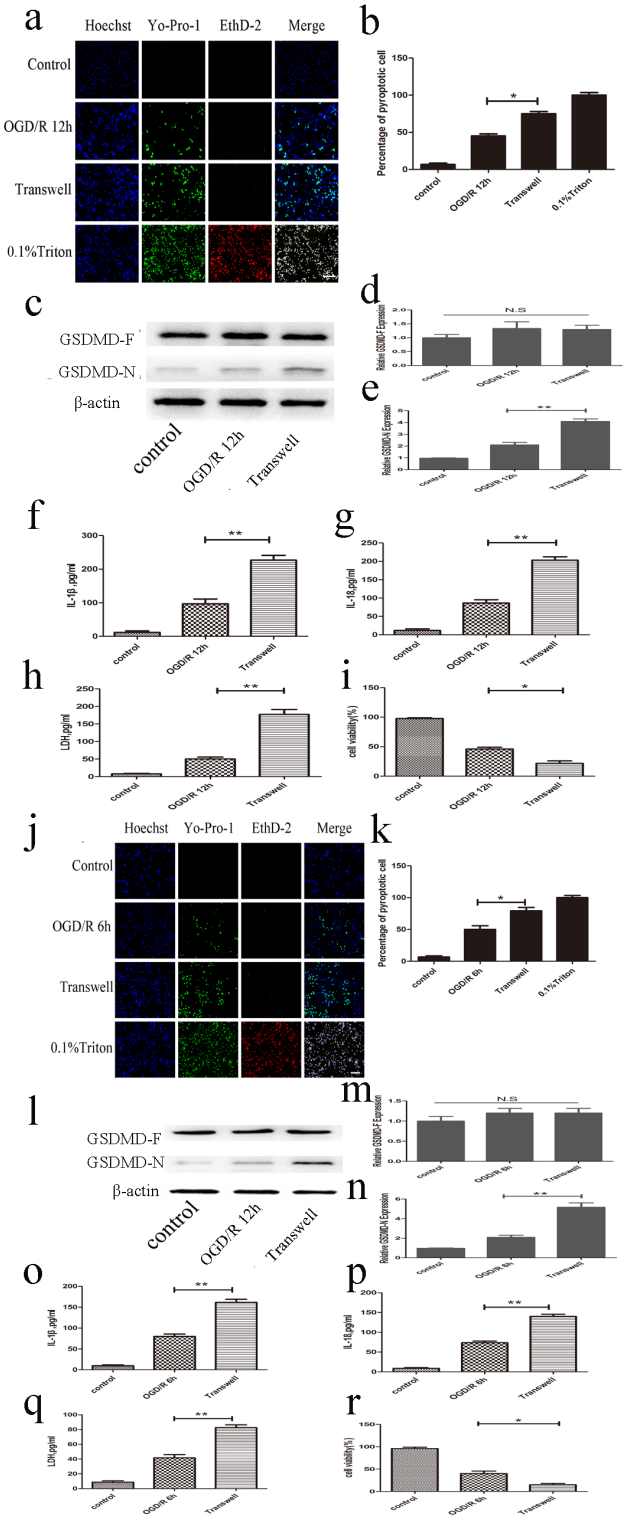

Figure 7

HT22 cells undergoing OGD/R aggravated pyroptosis of adjacent BV2 cells in the transwell co-culture model (as displayed in Figure 1)and vice versa. a and b. Representative immunofluorescence staining of BV2 cells by dye uptake method (a) and histogram of the percentage of pyroptotic BV2 cells (b). Compared with BV2 cells treated by OGD/R for 12h, there was greater pyroptotic proportion in BV2 cells which were plated in the lower layer of chamber and cultured with the solution of upper HT22 cells for

12h (indicated as Transwell in Figure). 0.1% Triton X-100 was used as a positive control. Magnification, ×100. Scale bar, 100um. c-e. Representative immunoblot and its quantification of GSDMD protein in BV2 cells. The GSDMD-N expression in Transwell BV2 cells was increased compared with that in BV2 cells treated by OGD/R for 12h. β-actin was used as a loading control. f-h. ELISA results showed that the level of IL-1β, IL-18 and LDH in cell supernatant of Transwell BV2 cells was increased compared with that in BV2 cells treated with OGD/R for 12h. i. The cell viability of Transwell BV2 cells was decreased compared with that of BV2 cells treated by OGD/R for 12h. j-k. Representative immunofluorescence staining of HT22 cells by dye uptake method (j) and histogram of the percentage of pyroptotic HT22 cells (k). Compared with HT22 cells treated by OGD/R for 6h, there was greater pyroptotic proportion in HT22 cells which were layed in the lower layer and cultured with the solution of upper BV2 cells for 6h (indicated as Transwell in Figure). 0.1% Triton X-100 was used as a positive control. Magnification, ×100. Scale bar, 100um. l-n. Representative immunoblot and its quantification of GSDMD protein in HT22 cells. The GSDMD-N expression in Transwell HT22 cells was increased compared with that in HT22 cells treated by OGD/R for 6h. β-actin was used as a loading control. o-q. ELISA results showed that the level of IL-1β, IL-18and LDH in cell supernatant of Transwell HT22 cells was increased compared with that in HT22 cells treated by OGD/R for 6h. R. The cell viability of Transwell HT22 cells was decreased compared with that in HT22 cells treated by OGD/R for 6h. All data were represented as mean ± SEM. n=3, *P<0.05, **P<0.01 compared with Transwell. N.S means nonsignificant difference.

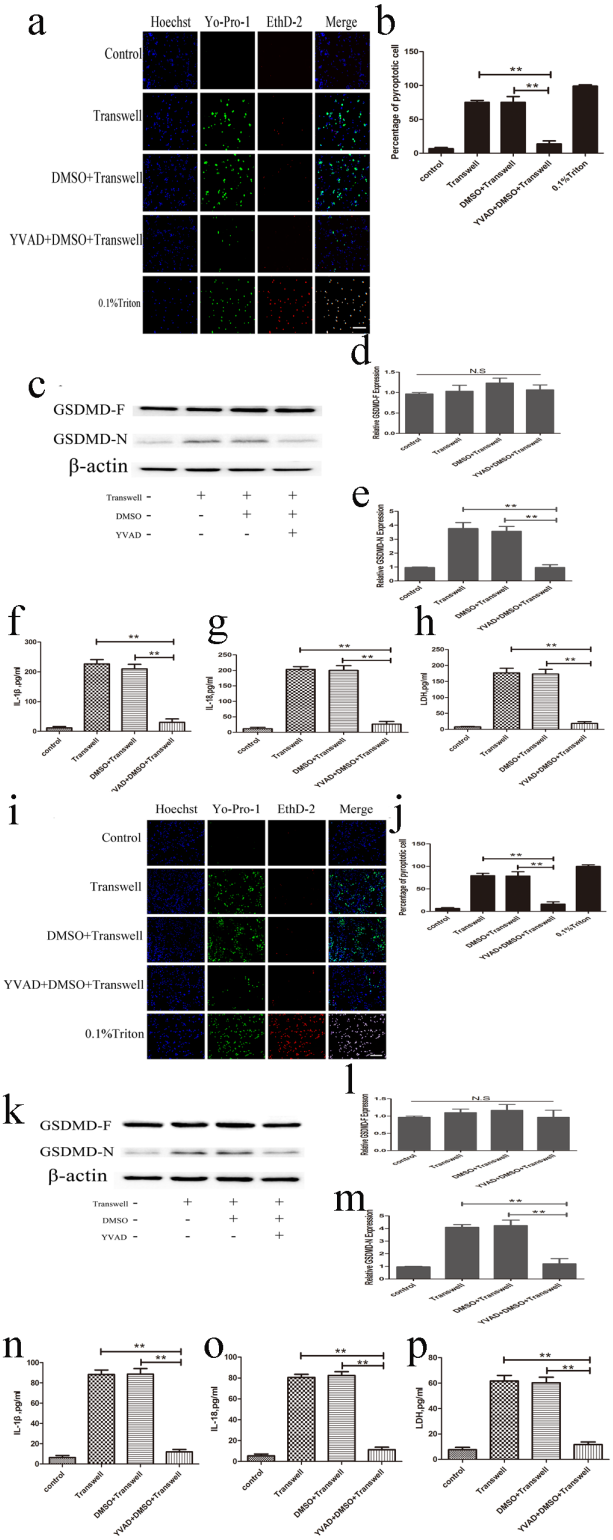

Figure 8

Inhibition of caspase-1 in HT22 cells before OGD/R alleviated pyroptosis of adjacent BV2 cells in the transwell co-culture model (as displayed in Figure 1), and vice versa. a and b. Representative immunofluorescence staining of BV2 cells by dye uptake method (a) and histogram of the percentage of pyroptoticBV2 cells (b). Compared with Transwell BV2 cells (as described in Figure 7), there was less pyroptotic proportion in BV2 cells which were plated in the lower layer and cultured for 12h with the

solution of upper HT22 cells pretreated with AC-YVAD-CMK (YVAD) before OGD/R (indicated as YVAD+DMSO+Transwell in Figure). 0.1% Triton X-100 was used as a positive control. Magnification, ×100. Scale bar, 100um. c-e. Representative immunoblot and its quantification of GSDMD protein in BV2 cells. The GSDMD-N expression in YVAD+DMSO+Transwell BV2 cells was decreased compared with that in Transwell BV2 cells. β-actin was used as a loading control. f-h. ELISA results showed that the level of IL-1β, IL-18 and LDH in cell supernatant of YVAD+DMSO+Transwell BV2 cells was decreased compared with Transwell BV2 cells. i-j. Representative immunofluorescence staining of HT22 cells by dye uptake method (i) and histogram of the percentage of pyroptoticBV2 cells (j). Compared with Transwell HT22 cells (as described in Figure 7), there was less pyroptotic proportion in HT22 cells which were layed in the lower layer and cultured for 6h with the solution of upper BV2 cells pretreated with YVAD before OGD/R (indicated as YVAD+DMSO+Transwell in Figure). 0.1% Triton X-100 was used as a positive control. Magnification, ×100. Scale bar, 100um. k-m. Representative immunoblot and its quantification of GSDMD protein in HT22 cells. The GSDMD-N expression in YVAD+DMSO+Transwell HT22 cells was decreased compared with that in Transwell HT22 cells. β-actin was used as a loading control. n-p. ELISA results showed that the level of IL-1β, IL-18 and LDH in cell supernatant of YVAD+DMSO+Transwell HT22 cells was decreased compared with that in Transwell HT22 cells. All data were represented as mean ± SEM. n=3, **P<0.01 compared with YVAD+DMSO+Transwell. N.S means nonsignificant difference.

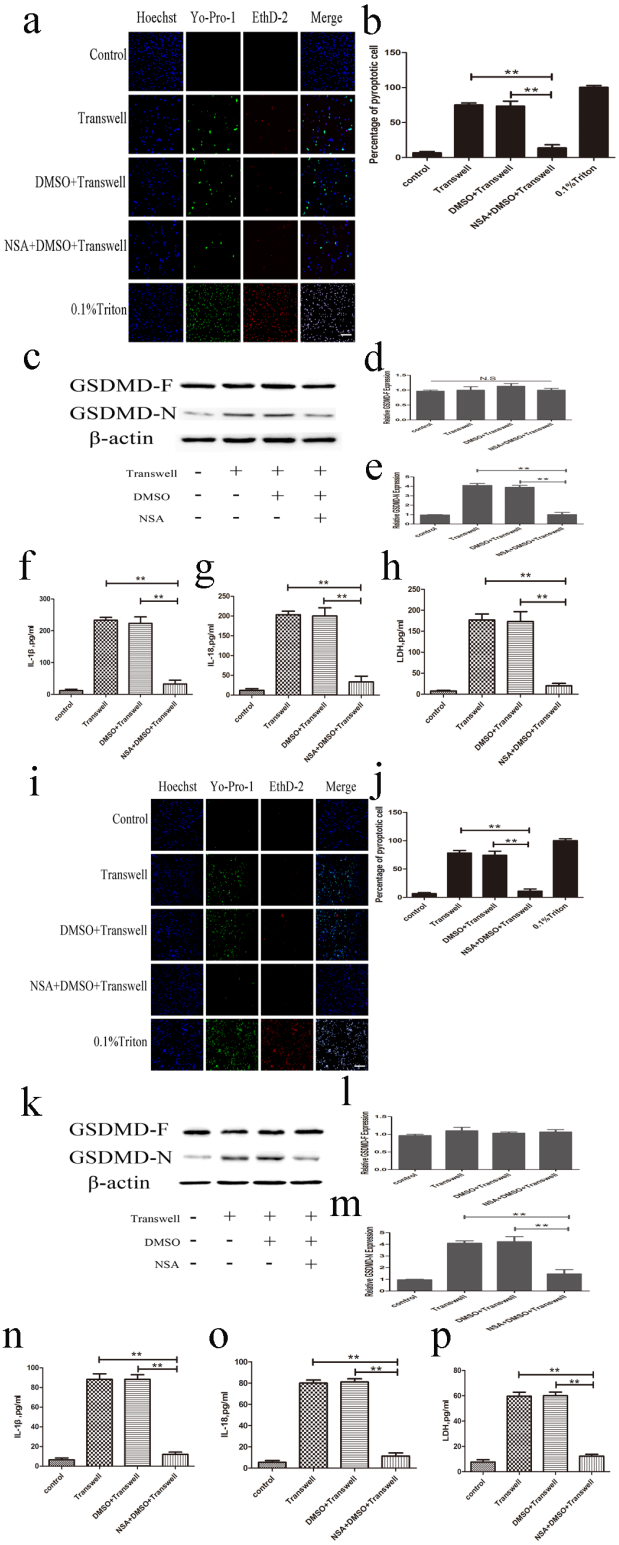

Figure 9

Inhibitionof GSDMD by necrosulfonamide (NSA) in HT22 cells before OGD/R alleviated pyroptosis of adjacent BV2 cells in the transwell co-culture model (as displayed in Figure 1), and vice versa. a and b. Representative immunofluorescence staining of BV2 cells by dye uptake method (a) and histogram of the percentage of pyroptotic BV2 cells (b). Compared with Transwell BV2 cells (as described in Figure 7), there was less pyroptotic proportion in BV2 cells which were layed in the lower layer and cultured for 12h

with the solution of upper HT22 cells pretreated with NSA before OGD/R (indicated as NSA+DMSO+Transwell in Figure). 0.1% Triton-X-100 was used as a positive control. Magnification, ×100. Scale bar, 100um. c-e. Representative immunoblot and its quantification of GSDMD protein in BV2 cells. The GSDMD-N expression in NSA+DMSO+Transwell BV2 cells was decreased compared with that in Transwell BV2 cells. β-actin was used as a loading control. f-h. ELISA results showed that the level of IL-1β, IL-18and LDH in cell supernatant of NSA+DMSO+Transwell BV2 cells was decreased compared with Transwell BV2 cells. i-j. Representative immunofluorescence staining of HT22 cells by dye uptake method (i) and histogram of the percentage of pyroptotic HT22 cells (j). Compared with Transwell HT22 cells (as described in Figure 7), there was less pyroptotic proportion in TH22 cells which were plated in the lower layer and cultured for 6h with the solution of upper BV2 cells pretreated with NSA before OGD/R (indicated as NSA+DMSO+Transwell in Figure). 0.1% Triton X-100 was used as a positive control. Magnification, ×100. Scale bar, 100um. k-m. Representative immunoblot and its quantification of GSDMD protein in HT22 cells. The GSDMD-N expression in NSA+DMSO+Transwell HT22 cells was decreased compared with that in Transwell HT22 cells. β-actin was used as a loading control. n-p. ELISA results showed that the level of IL-1β, IL-18 and LDH in cell supernatant of NSA+DMSO+Transwell HT22 cells was decreased compared with that in Transwell HT22 cells. All data were represented as mean ± SEM. n=3, **P<0.01 compared with NSA+DMSO+Transwell. N.S means nonsignificant difference.

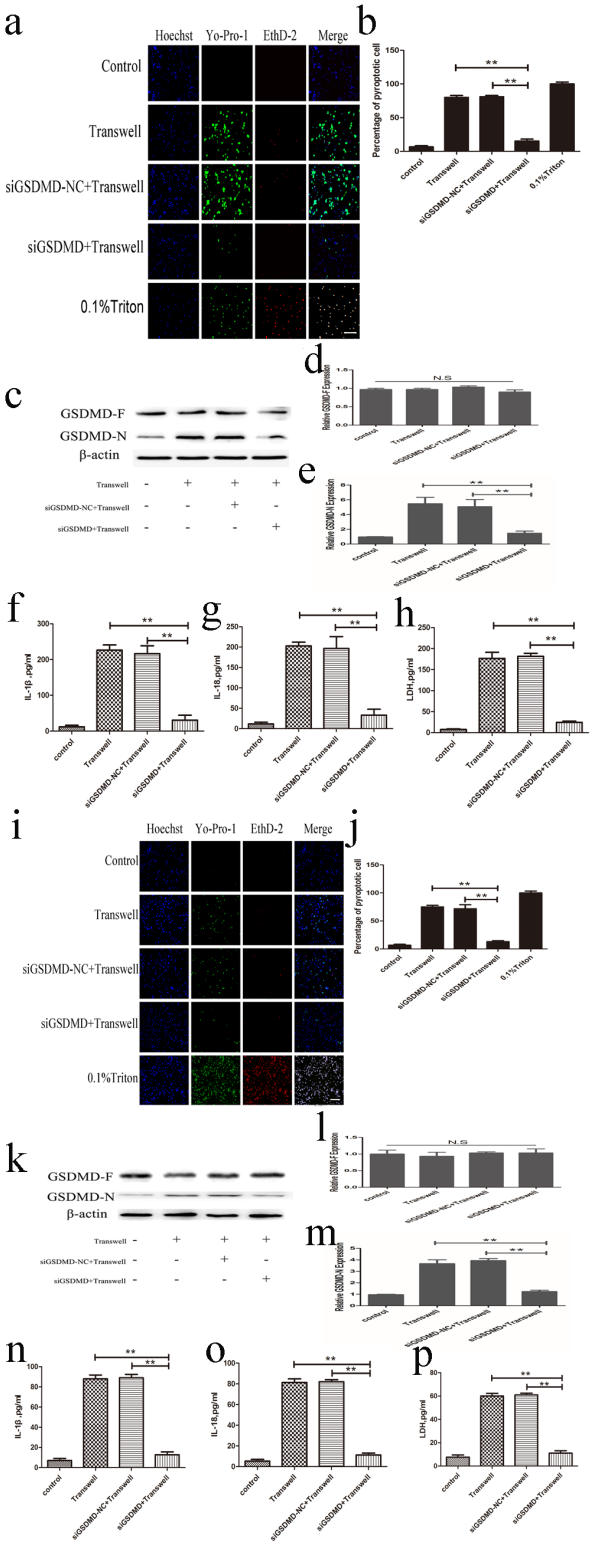

Figure 10

Knockdown GSDMD by siRNA in HT22 cells before OGD/R alleviated pyroptosis of adjacent BV2 cells in the transwell co-culture model (as displayed in Figure 1), and vice versa. a and b. Representative immunofluorescence staining of BV2 cells by dye uptake method (a) and histogram of the percentage of pyroptotic BV2 cells (b). Compared with Transwell BV2 cells (as described in Figure 7), there was less pyroptotic proportion in BV2 cells which were plated in the lower layer and cultured for 12h with the

solution of upper HT22 cells pretreated with siRNA of GSDMD（siGSDMD） before OGD/R (indicated as siGSDMD+Transwell in Figure). 0.1% Triton X-100 was used as a positive control. Magnification, ×100. Scale bar, 100um. c-e. Representative immunoblot and its quantification of GSDMD protein in BV2 cells. The GSDMD-N expression in siGSDMD+Transwell BV2 cells was decreased compared with that in Transwell BV2 cells. β-actin was used as a loading control. f-h. ELISA results showed that the level of IL-1β, IL-18 and LDH in cell supernatant of siGSDMD+Transwell BV2 cells was decreased compared with that in Transwell BV2 cells. i-j. Representative immunofluorescence staining of HT22 cells by dye uptake method (i) and histogram of the percentage of pyroptotic HT22 cells (j). Compared with Transwell HT22 cells (as described in Figure 7), there was less pyroptotic proportion in TH22 cells which were layed in the lower layer and cultured for 6h with the solution of upper BV2 cells pretreated with siGSDMD (indicated as siGSDMD+Transwell in Figure). 0.1% Triton X-100 was used as a positive control. Magnification, ×100. Scale bar, 100um. k-m. Representative immunoblot and its quantification of GSDMD protein in HT22 cells. The GSDMD-N expression in siGSDMD+Transwell HT22 cells was decreased compared with that in Transwell HT22 cells. β-actin was used as a loading control. n-p. ELISA results showed that the level of IL-1β, IL-18and LDH in cell supernatant of siGSDMD+Transwell HT22 cells was decreased compared with that in Transwell HT22 cells. All data were represented as mean ± SEM. n=3, **P<0.01 compared with siGSDMD+Transwell. N.S means nonsignificant difference.

Supplementary Files

This is a list of supplementary files associated with this preprint. Click to download.

- supplementalFig1.tif
- supplementalFig3.tif
- supplementalFig2.tif